Contents

1 Boundary-value problem and solution approach

The purpose of the NDSM code is to compute the magnetic vector potential $\boldsymbol{A}$ corresponding to a current-free (potential) field $\boldsymbol{B}$ in a Cartesian box. In addition, we require that normal component of $\boldsymbol{B}$ be imposed on the boundary of the box. The calculation of $\boldsymbol{A}$ has two stages. Firstly, the boundary conditions for $\boldsymbol{A}$ must be calculated from the given boundary conditions on $\boldsymbol{B}$. Secondly, the value of $\boldsymbol{A}$ in the volume is calculated.

The code is also described in [1].

1.1 Domain and boundary

The calculation is performed in a Cartesian box:

$$\Omega = \{(x, y, z) | 0 \leq x \leq L_x, 0 \leq y \leq L_y, 0 \leq z \leq L_z\}. \tag{1}$$

The boundary of the domain, $\partial\Omega$, consists of six planar faces S_i:

$$S_{x0} = \{(x, y, z) | x = 0, 0 \leq y \leq L_y, 0 \leq z \leq L_z\}, \tag{2}$$

$$S_{x1} = \{(x, y, z) | x = L_x, 0 \leq y \leq L_y, 0 \leq z \leq L_z\}, \tag{3}$$

$$S_{y0} = \{(x, y, z) | 0 \leq x \leq L_x, y = 0, 0 \leq z \leq L_z\}, \tag{4}$$

$$S_{y1} = \{(x, y, z) | 0 \leq x \leq L_x, y = L_y, 0 \leq z \leq L_z\}, \tag{5}$$

$$S_{z0} = \{(x, y, z)|0 \leq x \leq L_x, 0 \leq y \leq L_y, z = 0\}, \tag{6}$$

and

$$S_{z1} = \{(x, y, z)|0 \leq x \leq L_x, 0 \leq y \leq L_y, z = L_z\}. \tag{7}$$

The normal components on each face are the positive Cartesian unit vectors $\hat{\boldsymbol{x}}$,$\hat{\boldsymbol{y}}$, and $\hat{\boldsymbol{z}}$. Both the "upper" and "lower" boundaries have the same normal component.

In the code, the faces are numbered with a linear scheme:

$$(S_1, S_2, S_3, S_4, S_5, S_6) = (S_{x0}, S_{x1}, S_{y0}, S_{y1}, S_{z0}, S_{z1}) \tag{8}$$

1.2 Boundary-value problem for $\boldsymbol{A}$ in terms of b_n

In this section we describe the boundary-value problem for $\boldsymbol{A}$ in Ω in terms of the normal component of the magnetic field, b_n, at the boundary. This boundary-value problem is not in a standard Neumann/Dirichlet form and is not directly solved.

In the interior of Ω, let $\boldsymbol{A}$ satisfy the Coulomb gauge

$$\nabla \cdot \boldsymbol{A} = 0. \tag{9}$$

In this case, a current-free ($\boldsymbol{J} = 0$) magnetic field satisfies the vector Laplace equation

$$\nabla^2 \boldsymbol{A} = 0. \tag{10}$$

On the boundary $\partial\Omega$, we impose the boundary condition

$$(\nabla \times \boldsymbol{A}) \cdot \hat{\boldsymbol{n}} = b_n \tag{11}$$

Equations (10) - (11) define the boundary-value problem for $\boldsymbol{A}$.

The standard approach to formulating a boundary-value problem for the Laplace equation is in terms of either Dirichlet or Neumann boundary conditions [2]. In the context of computing $\boldsymbol{A}$, imposing Dirichlet conditions corresponds to imposing the transverse component of the vector potential:

$$\boldsymbol{A}_t|_{\partial\Omega} = (\boldsymbol{A} - \boldsymbol{A} \cdot \hat{\boldsymbol{n}})|_{\partial\Omega}\,, \tag{12}$$

and imposing Neumann conditions corresponds to imposing the normal derivative of the normal component:

$$\partial_n A_n|_{\partial\Omega} = \nabla(\boldsymbol{A} \cdot \hat{\boldsymbol{n}}) \cdot \hat{\boldsymbol{n}}|_{\partial\Omega}\,. \tag{13}$$

Equation (11) does not directly match either of these forms, and hence it is necessary to derive a set of Dirichlet/Neumann by first introducing addition gauge conditions at the boundary and secondly by solving a set of two-dimensional boundary-value problems at each boundary S_i. By this means, a set of boundary data for $\boldsymbol{A}_t$ and ∂A_n are derived that are consistent with Equation (11). We describe this process in Section 1.3.

1.3 Dirichlet/Neumann boundary conditions for $\boldsymbol{A}$

It is possible to introduce gauge conditions at the boundary to put the boundary-value problem described in Section 1.2 into a standard Dirichlet/Neumann form. First, however, we describe an approach to treating a "restricted" for of the boundary-value problem from Section 1.2. The "restricted" boundary-value problem requires b_n satisfies the compatibility condition

$$\int_{S_i} b_n \cdot \hat{\boldsymbol{n}} dS = 0, \tag{14}$$

for all six boundary faces S_{ij}. In other words, the restricted problem requires the net magnetic flux over each individual face to be zero.This is a much more restrictive condition than the requirement of net flux balance over the entire boundary, which should always be the case when $\nabla \cdot \boldsymbol{B} = 0$. This restriction turns out not to be a serious impediment, as it is not generally satisfied and limits the approach to a relatively uninteresting set of fields. In Section 1.5, however, we describe how the restricted approach can be made applicable to a generic magnetic field through the appropriate decomposition.

In addition to the Coulomb gauge condition, we follow [3] and impose the further condition

$$\nabla_i \cdot \boldsymbol{A}|_{\partial\Omega} = 0. \tag{15}$$

Here the operator $\nabla_i \cdot$ is a two-dimensional divergence operator defined on each face i. Given this constraint, it follows from Equations (9)-(11) that

$$\partial_n A_n = 0 \tag{16}$$

and

$$\boldsymbol{A}_t = \nabla_i \chi_i \times \hat{\boldsymbol{n}}, \tag{17}$$

where

$$\nabla_i^2 \chi_i = b_n|_{S_i}. \tag{18}$$

Here again, the subscript i indicates that the operator and variable is defined on the two dimensional boundary plane S_i.

1.4 Boundary-value problem for χ

The boundary condition on $\boldsymbol{A}_t$ is computed by solving Equation (18) on each boundary, subject to boundary conditions on each edge. Once choice of boundary condition is the homogeneous Neumann boundary condition

$$\partial_n \chi = 0. \tag{19}$$

This condition ensures that the gauge conditions are satisfied at the edges of the faces.

Equations (19) and (18) define the boundary value problem for χ on each face. Since the boundary conditions are homogeneous Neumann boundary conditions, the source

term in Equation (18) must satisfy a compatibility condition [4]. This condition is expressed by Equation (14).

For pure Neumann boundary-value problems the solution is only unique up to the addition of a constant, i.e. $\chi + c$ is also a solution. The lack of uniqueness does not affect the solution in principle, but in practice, it can make relaxation methods unstable. To ensure a unique solution, we enforce the further condition

$$\langle \chi_i \rangle = 0, \tag{20}$$

where $\langle\rangle$ is the average over S_i.

1.5 Decomposition and solution for a generic magnetic field

In this subsection we describe how to decompose a generic magnetic field so that problem of $\boldsymbol{A}$ reduces to solving the restricted boundary-value problem described in Section 1.3.

In order to satisfy the Neumann compatibility condition for a generic magnetic field, we decompose $\boldsymbol{A}$ as

$$\boldsymbol{A} = \boldsymbol{A}^{\mathrm{b}} + \boldsymbol{A}^{\mathrm{ub}}, \tag{21}$$

where both $\boldsymbol{A}^{\mathrm{b}}$ and $\boldsymbol{A}^{\mathrm{ub}}$ must satisfy Equations (10) and (9). We define $\boldsymbol{A}^{\mathrm{ub}}$ such that

$$\int_{S_i} (\nabla \times \boldsymbol{A}^{\mathrm{ub}}) \cdot \hat{\boldsymbol{n}} dS = \int_{S_i} b_n dS. \tag{22}$$

This condition ensures that

$$\int_{S_i} (\nabla \times \boldsymbol{A}^{\mathrm{b}}) \cdot \hat{\boldsymbol{n}} dS = \int_{S_i} b_n^{\mathrm{b}} dS = 0 \tag{23}$$

over each boundary face. The vector potential and magnetic field $\boldsymbol{A}^{\mathrm{ub}}$ and $\boldsymbol{B}^{\mathrm{ub}}$ are not uniquely defined by Equation (23). It is convenient, however, to use a version of $\boldsymbol{A}^{\mathrm{ub}}$ that has a simple analytic form. This way it is not necessary to expend effort computing it numerically. A suitable form for $\boldsymbol{A}^{\mathrm{ub}}$ and therefore $\boldsymbol{B}^{\mathrm{ub}}$ is given in Appendix A.

Given $\boldsymbol{B}^{\mathrm{ub}}$, we may define a corrected magnetic normal component

$$\boldsymbol{B}^{\mathrm{b}} \cdot \hat{\boldsymbol{n}} = b_n - \boldsymbol{B}^{\mathrm{ub}} \cdot \hat{\boldsymbol{n}}. \tag{24}$$

The vector potential $\boldsymbol{A}^{\mathrm{b}}$ can then be found by the method of Section 1.3 with $\boldsymbol{B}^{\mathrm{b}} \cdot \hat{\boldsymbol{n}}$ as the right-hand side of Equation 18. By construction of $\boldsymbol{B}^{\mathrm{ub}}$, the Neumann compatibility condition is satisfied for $\boldsymbol{B}^{\mathrm{b}} \cdot \hat{\boldsymbol{n}}$

2 Definitions of $\boldsymbol{A}^{\mathrm{ub}}$ and $\boldsymbol{B}^{\mathrm{ub}}$

2.1 Vector potential: $\boldsymbol{A}^{\mathrm{ub}}$

In this section we give the analytic form of the vector potential $\boldsymbol{A}^{\mathrm{ub}}$. It is convenient to define the following:

$$\gamma_x = \frac{\Phi_{x1} - \Phi_{x0}}{V}, \tag{25}$$

$$\gamma_y = \frac{\Phi_{y1} - \Phi_{y0}}{V}, \tag{26}$$

and

$$\gamma_z = \frac{\Phi_{z1} - \Phi_{z0}}{V}. \tag{27}$$

Here Φ_i is the flux over each boundary S_i:

$$\Phi_i = \int_{S_i} \boldsymbol{B}_c \cdot \hat{\boldsymbol{n}} dS, \tag{28}$$

and

$$V = L_x L_y L_z. \tag{29}$$

When defining the flux, we use the same normal on both the "lower" and "upper" boundaries, e.g. the positive unit vector $\hat{\boldsymbol{z}}$ is used on both the $z = 0$ and $z = L_z$ surfaces. With this choice, the variables γ_i are the net flux entering and exiting in a particular dimension divided by the total volume of the domain.

The vector potential $\boldsymbol{A}^{\mathrm{ub}}$ that corresponds to $\boldsymbol{B}^{\mathrm{ub}}$ can be expressed as a sum

$$\boldsymbol{A}^{\mathrm{ub}} = \boldsymbol{A}^{\mathrm{ub}}_{\mathrm{L}} + \boldsymbol{A}^{\mathrm{ub}}_{\mathrm{BL}}. \tag{30}$$

The first term is linear in x, y and z and is given by

$$\boldsymbol{A}^{\mathrm{ub}}_{\mathrm{L}} = -\left(\frac{\Phi_{x0} L_x}{V}\right) x\hat{\boldsymbol{x}} - \left(\frac{\Phi_{y0} L_y}{V}\right) y\hat{\boldsymbol{y}} - \left(\frac{\Phi_{z0} L_z}{V}\right) z\hat{\boldsymbol{z}}. \tag{31}$$

The second term is bilinear in terms of the pairs xy, xz, and yz, and it is formed by linear combinations of the terms

$$\boldsymbol{A}^{\mathrm{ub}}_1 = -\gamma_z yz\hat{\boldsymbol{x}} + \gamma_x xy\hat{\boldsymbol{z}}, \tag{32}$$

$$\boldsymbol{A}^{\mathrm{ub}}_2 = -\gamma_x xz\hat{\boldsymbol{y}} + \gamma_y zy\hat{\boldsymbol{x}}, \tag{33}$$

and

$$\boldsymbol{A}^{\mathrm{ub}}_3 = -\gamma_y xy\hat{\boldsymbol{z}} + \gamma_z xz\hat{\boldsymbol{y}}. \tag{34}$$

Older versions of the NDSM code use

$$\boldsymbol{A}^{\mathrm{ub}}_{\mathrm{BL}} = \boldsymbol{A}_2. \tag{35}$$

Later versions use

$$\boldsymbol{A}^{\mathrm{ub}}_{\mathrm{BL}} = \frac{\boldsymbol{A}^{\mathrm{ub}}_1 + \boldsymbol{A}^{\mathrm{ub}}_2 + \boldsymbol{A}^{\mathrm{ub}}_3}{3}. \tag{36}$$

This second form is preferred because it does not privilege any particular direction. Both forms are related by a gauge transformation and both correspond to the same magnetic field.

2.2 Magnetic field: $\boldsymbol{B}^{\mathrm{ub}}$

The magnetic field $\boldsymbol{B}^{\mathrm{ub}}$ that corresponds to the vector potential $\boldsymbol{A}^{\mathrm{ub}}$ has components

$$\boldsymbol{B}^{\mathrm{ub}}_x = \frac{(L_x - x)\Phi_{x0} + \Phi_{x1}x}{V}, \tag{37}$$

$$\boldsymbol{B}^{\mathrm{ub}}_y = \frac{(L_y - y)\Phi_{y0} + \Phi_{y1}y}{V}, \tag{38}$$

and

$$\boldsymbol{B}^{\mathrm{ub}}_z = \frac{(L_z - z)\Phi_{z0} + \Phi_{z1}z}{V}. \tag{39}$$

The divergence of this magnetic field is

$$\nabla \cdot \boldsymbol{B}^{\mathrm{ub}} = \frac{\Phi_{x1} - \Phi_{x0} + \Phi_{y1} - \Phi_{y0} + \Phi_{z1} - \Phi_{z0}}{V}, \tag{40}$$

and it follows that $\nabla \cdot \boldsymbol{B}^{\mathrm{ub}} = 0$ when there is net flux balance over the entire boundary $\partial\Omega$, which is a basic requirement for any magnetic field [5].

It is instructive to split $\boldsymbol{B}$ into two terms that correspond to the two terms of $\boldsymbol{A}^{\mathrm{ub}}$, i.e.

$$\boldsymbol{B}^{\mathrm{ub}} = \boldsymbol{B}^{\mathrm{ub}}_{\mathrm{L}} + \boldsymbol{B}^{\mathrm{ub}}_{\mathrm{BL}}. \tag{41}$$

The first terms is

$$\boldsymbol{B}^{\mathrm{ub}}_{\mathrm{L}} = \left(\frac{L_x}{V}\right)\hat{\boldsymbol{x}} + \left(\frac{L_y}{V}\right)\hat{\boldsymbol{y}} + \left(\frac{L_z}{V}\right)\hat{\boldsymbol{z}}, \tag{42}$$

and is constant. The second term is

$$\boldsymbol{B}^{\mathrm{ub}}_{\mathrm{LB}} = \gamma_x x\hat{\boldsymbol{x}} + \gamma_y y\hat{\boldsymbol{y}} + \gamma_z z\hat{\boldsymbol{z}} \tag{43}$$

and is linear in x, y, and z.

3 Summary of the algorithm

In this section we summarize the algorithim.

1. Compute $\boldsymbol{A}^{\mathrm{ub}}$ and $\boldsymbol{B}^{\mathrm{ub}}$ analytically from $\boldsymbol{B}_c \cdot \hat{\boldsymbol{n}}$.
2. Compute $\boldsymbol{B}^{\mathrm{b}} \cdot \hat{\boldsymbol{n}}$ on the $\partial\Omega$ from Equation (24)

3. Compute $\boldsymbol{A}_t^{\mathrm{b}}$ on each face by solving Equation (18) on each face S_i
4. Compute $\boldsymbol{A}^{\mathrm{b}}$ by solving the vector Laplace equation with boundary conditions given by Equation (16)-(17)
5. Compute the resultant field $\boldsymbol{A} = \boldsymbol{A}^{\mathrm{ub}} + \boldsymbol{A}^{\mathrm{b}}$.

4 Numerical implementation

In this section we describe the numerical implementation of the algorithim.

The two-dimensional and three-dimensional boundary-value problems discretized using a second-order centered difference approximation. The finite-difference equations are solved using a geometric multigrid method based on a Red-Black relaxation operator. Linear interpolation and full-weighted restriction are used for prorogation and restriction.

Multigrid V cycling in used to solve the system of equations. The cycling is halted when the maximum difference between iterations is below a given threshold. We typically use a value of order 10^{-12}.

5 Test results

We apply the code to a set of test cases with known solutions. The figures in this section show error metric versus mesh spacing h.

5.1 Integration tests: truncation error scaling

The first integration test measures the truncation error scaling for both $\boldsymbol{A}$ and $\boldsymbol{B}$ by applying the code to a known (analytic) test case. Generally, the truncation error for finite-difference method has a power-law form, i.e.

$$E_{\mathrm{error}} = Ah^{\gamma}, \tag{44}$$

where h is the mesh spacing, and A and γ are constants. The NDSM code is based on a second-order scheme, so we expect $\gamma \approx 2$ for NDSM. Therefore, the criterion for a successful test is getting a measured value of γ close to this theoretical value. Note that $\gamma = 2$ is technically the asymptotic scaling, and for large mesh spacing, departure from this value is expected.

The truncation error scaling is an example of a convergence metric – it measures the convergence of the numerical scheme to the idealized continuous limit $h \to 0$. Such metrics are generally a more rigorous test of the correctness of the implementation than

simply showing that error is small for a fixed mesh spacing.A departure from the correct scaling can indicate problems with the implementation of boundary conditions for example, that may not be obvious when performing a calculation at one mesh scale.

5.1.1 Truncation error metrics

To estimate the truncation error, we can apply the code to a known test case and estimate the error using standard metrics

$$E_{\max} = \max(||\boldsymbol{V}_1 - \boldsymbol{V}_2||) \tag{45}$$

and

$$E_{\text{avg}} = \langle ||\boldsymbol{V}_1 - \boldsymbol{V}_2|| \rangle, \tag{46}$$

where $\boldsymbol{V}_1$ and $\boldsymbol{V}_2$ are two vector fields. The operator $||.||$ is the standard vector norm.

5.1.2 Test case 1

The first test measures the truncation error scaling for both $\boldsymbol{A}$ and $\boldsymbol{B}$. Here we first describe the analytic test case, and then the results.

The test case is a magnetic potential field with components

$$B_x = l \sin(kx) \cos(ky) \exp(-lz), \tag{47}$$

$$B_y = l \cos(kx) \sin(ky) \exp(-lz), \tag{48}$$

and

$$B_z = 2k \cos(kx) \cos(ky) \exp(-lz), \tag{49}$$

where k is in principle a "free parameter", but for comparisons involving the vector potential it must be chosen as πn, where n is an integer, to ensure the boundary condition $\partial_n A_n = 0$ is satisfied. The other parameter, l, is computed from k as $l = \sqrt{2}k$. This choice of l is necessary for the magnetic field to have zero divergence.

The vector potential has components

$$A_x = -\cos(kx) \sin(ky) \exp(-lz), \tag{50}$$

$$A_y = +\sin(kx) \cos(ky) \exp(-lz), \tag{51}$$

and

$$A_z = 0. \tag{52}$$

Only when $k = \pi n$ is this as suitable test case for comparison with the NDSM code. When k is chosen otherwise, $\boldsymbol{A}$ does not satisfy the boundary condition $\partial_n A_n = 0$.

The results are shown in Figure 1. The left panel shows the truncator error metrics for the vector potential and the right shows the same for the magnetic field. The solid lines indicate power-law fits to the data. In all four cases the power-law index, γ, is close to the theoretical value of $\gamma = 2$. The truncation error for $\boldsymbol{B}$ is generally larger and magnitude. The magnetic field is computed as the curl of $\boldsymbol{A}$ numerically, and which is an additional source of error on top of the error introduced via the solution method itself.

It is also interesting to measure the run time as a function of the problem size. We can use N, the number of mesh points in each dimension, as a basic measure of the problem size. With this definition of N, the total number of mesh points in three-dimensions is then N^3. Figure 2 shows the measured runtimes, t, versus N. The solid line is a power-law fit to the data with a power-law index of $\gamma \approx 2.6$. The ideal multigrid scaling is $t \sim N^3$. The measured scaling is less than this. The code, however, is not really achieving a scaling better than the ideal, instead the fit is affected by the values at small N, which benefit from a speedup due to caching etc. and do not reflect performance at larger mesh sizes. When these points are excluded, the scaling is closer to $\gamma = 3$.

References

[1] K. E. Yang, M. S. Wheatland, and S. A. Gilchrist, "Relative Magnetic Helicity Based on a Periodic Potential Field," *The Astrophysical Journal*, vol. 894, p. 151, May 2020.

[2] P. Morse and H. Feshbach, *Methods of theoretical physics*. International series in pure and applied physics, McGraw-Hill, 1953.

[3] T. Amari, T. Z. Boulmezaoud, and Z. Mikic, "An iterative method for the reconstructionbreak of the solar coronal magnetic field. I. Method for regular solutions," *Astron. Astrophys.*, vol. 350, pp. 1051–1059, Oct 1999.

[4] W. L. Briggs, V. E. Henson, and S. F. McCormick, *A Multigrid Tutorial (2Nd Ed.)*. Philadelphia, PA, USA: Society for Industrial and Applied Mathematics, 2000.

[5] J. D. Jackson, *Classical Electrodynamics, 3rd Edition*. July 1998.

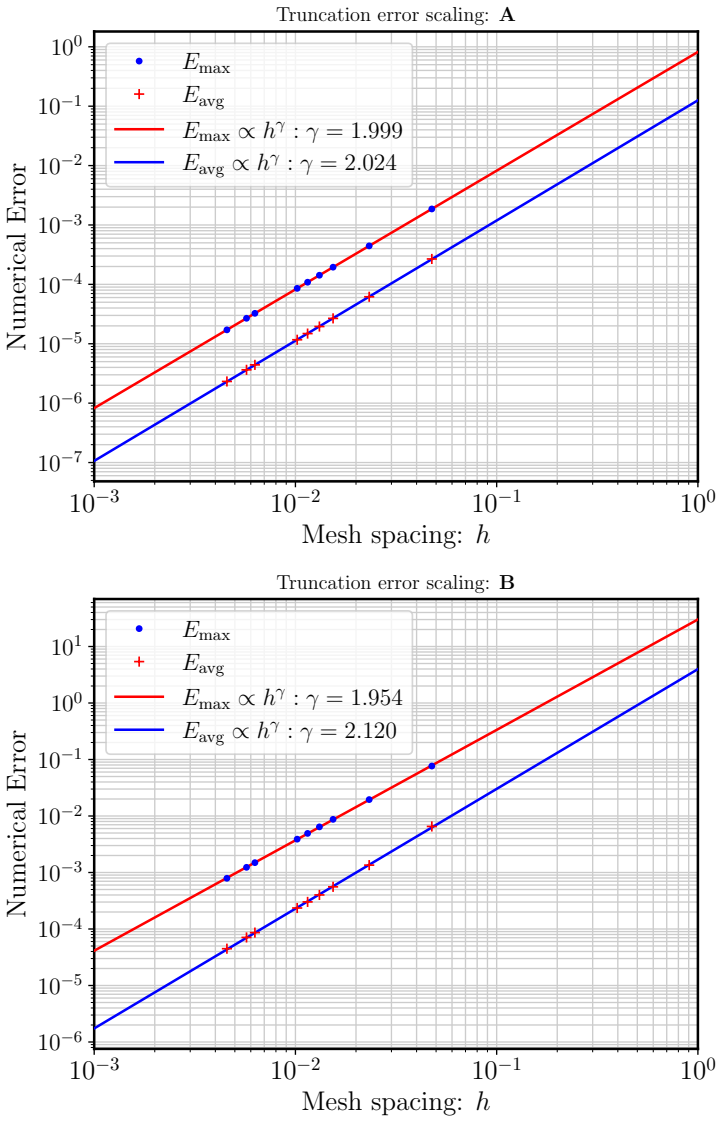

Figure 1: Truncation error scaling for the test case described in Section 5.1.2. The solid lines are power-law fits to the data.

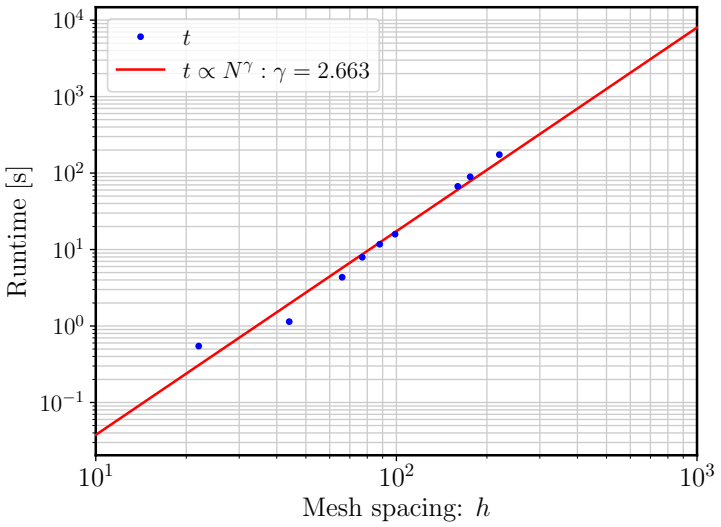

Figure 2: Time to calculate solution versus number of mesh points in each dimension N. The total number of mesh points is N^3. The ideal multigrid scaling is $t \sim N^3$.